Solid State Phenomena Vols. 99-100 (2004) pp 181-190
Online available since 2004/Jul/31 at www.scientific.net

doi:10.4028/www.scientific.net/SSP.99-100.181

Recent Developments in the Synthesis of Iron-based Nanostructures by Laser Pyrolysis: Integrating Structural Analysis with the Experimental Method.

R. Alexandrescu, I. Morjan, F. Dumitrache, I. Voicu, I. Soare, I. Sandu and C.T. Fleaca

National Institute for Lasers, Plasma and Radiation Physics, Laser Department, P.O. Box MG-36, R-76900 Bucharest, Romania

Keywords: Laser pyrolysis, nanoparticle, nanotechnology, iron pentacarbonyl

Abstract. The paper briefly reviews some fundamental and applicative characteristics of the laser pyrolysis technique. Recent developments of this method for the synthesis of iron-based nanostructures are emphasized. By varying the precursor gas mixture, iron/carbon nanocomposites (core-shell structures) and gamma iron oxide nanopowders were obtained and characterized. Novel structural features of the synthesized titanium-doped nano iron oxides are described.

Introduction

The CO_2 laser pyrolysis of gas phase reactants provides a powerful and versatile tool for producing nanostructures of various compositions. Very pure nano-scale materials when reaction occurs in the gas phase, far from polluting walls, may be prepared. The properties and structures are controlled by the main process parameters (precursor gas (vapour), gas flow rate, pressure, laser power.

Iron-based materials have a huge number of applications: magnetic storage media, sensors, catalysts etc. New approaches to their functionality are opened if particles in the nanometer size range are used. We present comprehensive investigations of different iron-based nano-phase compounds prepared by laser pyrolysis. Sensitized iron pentacarbonyl-based mixtures were used. Various structural characteristics of the reaction products were revealed: gamma iron oxides, iron-carbon core-shell structures and titanium doped iron oxides composites. Mean size diameters ranging from 1.5 to 9 nm and sharp particle distributions were often obtained. The combined results of several analytical methods (TEM, HREM, EELS, XRD, IR and Raman spectroscopy, thermal analysis) were used to define and characterize such nanostructures..

Basic fundamental and experimental features of laser pyrolysis from gas phase

Nanoparticles synthesis by laser pyrolysis was pioneered at MIT in 1982 by the group of Haggerty and Cannon [1]. Most work performed in the following years was devoted to the synthesis of silicon and Si-based compounds (Si, SiC, Si/C/N, Si_3N_4) [2-10]. The laser pyrolysis technique allows for the preparation of a large variety of nanosized bodies (with diameters ranging from a few nm to about 100 nm) by promoting IR laser-induced reactions in the gas phase.

Involved photochemistry and mechanism. The basic principles of the laser pyrolysis method rely on IR photochemistry, namely i) resonant absorption of photons by IR-active vibrational modes of molecules in ground electronic state; ii) collision-aided vibrational energy transfer towards the translation-rotation degrees of freedom and iii) heating of the reactant gases and dissociation, followed by nucleation and growth of aggregates. In any environment where multiple collisions occur on the time scale of a chemical reaction, the vibrational modes of a polyatomic molecule will equilibrate, and reaction occurs without energy localization in a single mode [11]

Laser pyrolysis is based on the overlapping of the emission line of the laser with an absorption line of one or more precursors. The 10P(20) CO_2 laser line peaks at 10.591 μm and is the strongest emission line. An additional substance, the so-called sensitizer is used in the case of non-absorbing gas precursors. It absorbs the energy and transmits it to the precursors by collisions. As a final effect of a laser-absorbing system coupling, the laser acts as a heat source. Under the conditions of laser intensity and gas pressure, the time between absorption of photons by the reactant gases is much greater than that necessary for distribution of the energy to local gas molecules through collisions thus, they are in thermal equilibrium. In this case, only one of the gas species needs to absorb the laser energy, since the others will be heated by collisions. This response is in marked contrast to unimolecular, multiphoton reactions where each gas molecule absorbs enough energy to cause dissociation before colliding with other gas molecules in the system, thus precluding a "thermal" reaction [1,2]

Process description. The system is based on a cross-flow configuration. The reactant flow emerges in the reactor through a nozzle system where it is orthogonally intersected by the focused IR radiation beam. Pyrolysis in the gas phase occurs in the small volume defined by the radiation-gases crossing where usually a "flame" appears. It is believed that the visible emission is primarily thermal, resulting from the hot particles [1]. The confinement of gas precursors toward the flow axis and of the freshly nucleated particles is achieved by a coaxial argon flow. Nucleated particles are kept entrained by the gas stream and collected in a removable tank at the reaction cell exit. Alternatively, the particles may be deposited on a substrate positioned in the flow reactor. The main process parameters are: the nature of the gas (vapor) precursors, gas flow rate, pressure as well as laser wavelength and power. For liquid precursors, the bubbled vapours are carried into the reaction zone by a carrier gas. By directing the laser beam onto a substrate, the pyrolysis of gas-phase molecules occurs on contact with a heated surface and patterned nanostructures may be grown.

Particle growth. Once the reactant gases reach the reaction temperature, particles begin to nucleate and grow in the gas stream. Particle nucleation and growth are complex processes, which usually depend on reaction pathways given by the specific experimental conditions (particularly the nature and number of reactants). For some particular reaction (involving silane as gas precursor), the laser-heated gas decomposes into silicon dimmers and trimers [1,2]. Particles grow by collisions (the growth is proportional to the system pressure) and non-dispersible aggregates are formed. Agglomerates form once sintering rates can no longer form dense, spherical particles in the time interval between collisions. In the case of silicon carbide formation, first silane decomposes; solid Si particles start to grow by collisions and coalesce in a hydrocarbon atmosphere. As they reach the temperature zone of about 1600^0 C carburisation becomes rapid (the temperature increases due to exothermic carburisation reaction and by increased CO_2 laser absorption by the SiC particles) [1,2].

Rice and co-workers [6] analysed particle formation from large organometallic molecules, for example, $(Me_3Si)_2$ NH. Taking into account the relative bond strengths, the pyrolysis products are consistent with a free radical mechanism whereby methyl radicals are generated initially, with the subsequent generation of larger radical species and methane. The overall mechanism is particle formation via molecular weight growth in which sequential addition steps produce increasingly large molecules and radicals until the reactions are quenched or until radicals are exhausted.

Granquist and co-workers [12] proposed a model in which the formation of nanoparticles in the gas phase requires a supersaturated vapour of monomers (atoms, molecules or fragments which support the growth) This leads to homogeneous nucleation. The nuclei must exceed a critical diameter to be stable. The growth continues by adsorption of atoms, or molecules, onto the nanoparticle or by

coalescence or coagulation due to collisions between nanoparticles Log-normal size dependence for particles grown under coalescence have been found.

Advantages and drawbacks. The clear advantage of laser pyrolysis over competing techniques is the high versatility that allows the production of a wide range of nanopowders. Among others, besides Si-based compounds [1-10], fullerenes [13-15], titanium and aluminum based compounds [16,17], nanocarbons [18], carbon nitride [19], carbon nanotubes [20], iron [21-23], iron oxides [24,25], iron carbides [26,23], iron-carbon nanocomposites [27,28] and titanium-doped iron oxides [29] were produced.

Laser pyrolysis from the gas phase is a vapour phase method of synthesis where the reactants are dilute and therefore yield a fine, loosely agglomerated powder, narrow particle size distributions, and controlled purity [1]. Unlike furnace-heated, rf-heated and arc-plasma-heated gas-phase synthesis techniques laser pyrolysis develops almost ideal thermal profiles and a reaction zone which permits uniform nucleation and growth. The efficiency of the technique is high: when optimised, the overall process efficiency is essentially that of conversion of electrical energy to laser light, ~ 15% for CO_2 lasers used [1-5]. Due to the lack of contact with surfaces (reactor hot walls) particles of high purity may be prepared. The homogeneous nucleation of molecules and the variable reaction conditions enable control of growth rate and time in the reaction zone. This allows extremely fine powders, often about 10 nm diameter, of small size distribution to be otained.

The drawbacks of the laser pyrolysis technique are the constraints imposed on the reactants [6]: the desired elements must be present in a vapour phase and at least one reactant must contain an infrared absorption band for coupling the energy with the laser beam.

Laser pyrolysis of gas mixtures containing iron pentacarbonyl: mechanism and experimental devices. $Fe(CO)_5$ is one of the most used metal carbonyls for precursors in conventional CVD or in photolytically or thermally laser-induced processes [30]. Like other metal carbonyls, $Fe(CO)_5$ molecules meet also other prerequisites for CVD, like stability and relevant vapour pressure at room temperature (around 25 torr at 300 K). A study dedicated to iron nanoparticles prepared by thermal decarbonylation of $Fe(CO)_5$ indicates that the primary photochemical event is believed to be ejection of CO to form $Fe(C0)_4$ which is then free to participate in further reactions such as cluster formation [31]:

$$Fe(CO)_4 + Fe(CO)_5 = Fe_2(CO)_9. \quad (1)$$

Addition of more $Fe(CO)_4$ radicals to produce larger clusters is known to occur, but only when the reaction mixture is overheated and then only a small yield. Under normal photolytic conditions the dimer concentration is limited by the fact that metal-metal bond scission is likely the favoured primary process. Ultimately, this will lead to the decomposition of $Fe(CO)_5$ to produce bulk metallic iron and CO gas. For pure photolytic processes, a recent model [32] estimates the proportion of unsaturated fragments, which will then depend on the photolysis wavelength and laser intensity, since multiphoton processes can also be involved.

Studies of $Fe(CO)_5$ sequential decarbonylation by laser pyrolysis [33] revealed the fast removal of carbonyl ligands (first bond energy of 41.5 Kcal/mol), with the formation of metallic iron and CO:

$$Fe(CO)_5 = Fe(CO)_x + (5-x)CO, \; x = 0 - 4. \quad (2)$$

In the sensitized CO_2 laser pyrolysis of $Fe(CO)_5$ the IR radiation is used to heat an absorbing gas called sensitizer (SF_6 or C_2H_4) which then collisionally transfers its vibrational energy to the

$Fe(CO)_5$ molecules to make them decompose (the absorption coefficients of SF_6 and C_2H_4 at the laser radiation wavelength of the usual CO2 lasers are 0.2 $torr^{-1}cm^{-1}$ and 1.7x 10^{-3} $torr^{-1}$ cm^{-1}, respectively). Many reports indicate that, in the case of $Fe(CO)_5$ gas-phase decomposition, the rate-determining process is the first decarbonylation of the thermally excited $Fe(CO)_5$ into $Fe(C0)_4$ and CO: it was observed [34] that further decarbonylation from $Fe(CO)_{5-m}$ (m=1-4) to $Fe(CO)_{4-m}$ and CO proceeds rapidly due to the weaker remaining bonds. The final products of the fast decarbonylation should be CO and iron particles, but the decomposition yield will obviously depend on the reaction temperature, which in turn is determined by the irradiation parameters.

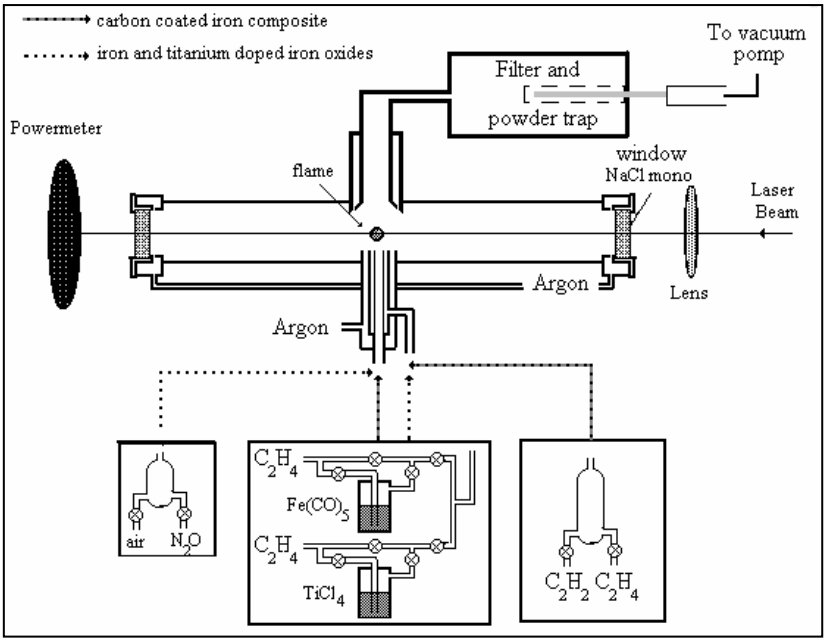

Fig. 1. General-purposes laser pyrolysis installation for the synthesis of iron-based compounds

In this paper, examples of laser pyrolysis processes of $Fe(CO)_5$-based gas mixtures, partly relying on our previous reported results, will be presented in a sequence relevant for the phenomenology of the process and the nanopowder structure characterization. Some characteristics of the laser-sensitized pyrolysis for producing iron oxides in the gamma phase will be discussed. Using $Fe(CO)_5$ in a mixture with hydrocarbon precursors and a particular irradiation geometry, iron particles embedded in carbon sheets were obtained. Finally, new results on the synthesis of titanium-doped iron oxides are presented. From an experimental point of view in each of these systems the laser pyrolysis installation was adapted to the demands of the specific conditions, mainly imposed by the nature of the precursors and the final aim of the synthesis process. In Fig. 1, a schematic general-purposes laser pyrolysis installation is depicted. The detailed description of the process corresponds to that presented previously. The CW CO_2 laser delivered a nominal power of 100 Watt. The variable trend concerns the different gas flows through the triple nozzle system. For instance, in the case of iron oxides and titanium doped iron oxides, air/N_2O (as oxidizers) flow through the inner nozzle tube while the middle tube allows entry of $Fe(CO)_5$/ $TiCl_4$ vapours, carried by C_2H_4. Inversely, for iron-carbon core-shell structures, iron pentacarbonyl flows through the inner tube while the mixture of hydrocarbon precursors (C_2H_2 and C_2H_4) is surrounds the central gas stream by flowing through the middle tube.

Iron-based nano powders synthesized by laser pyrolysis.

Gamma iron oxide nanopowders. The continuous [35, 37 ,24] laser pyrolysis technique was used for the preparation of iron oxide nanoparticles. Some representative results for the synthesis of

gamma iron oxides by the CO_2 CW laser pyrolysis [24,25] are presented. Using the cross-flow configuration shown in Fig.1, the laser beam orthogonally intersects the gas stream emerging from a double-nozzle configuration system. The reactive mixture consisting of $Fe(CO)_5$ vapours (carried by the sensitizer (either C_2H_4 or SF_6)) and of the oxidizing agent – usually air was crossing the inner tube. The experimental parameters for two representative runs are presented in Table 1. The total argon flow (for gas confinement and window cleaning) was kept at 1.3 l/min. In all runs the CO_2 laser power was 100 Watt

Run	Carrier gas	$\phi_{carrier}$ [sccm]	ϕ_{Air} [l/min]	P [torr]
V	SF_6	8	0.5	150
VI	C_2H_4	250	0.5	152

Table 1. Experimental parameters for the synthesis of iron oxides

Pure γ-iron oxide particles of nanometric size were obtained from. $Fe(CO)_5$/air/C_2H_4 mixtures (i.e. using C_2H_4 as sensitizer) (see Table 1). In powders marked VI, SF_6 sensitizer was replaced with C_2H_4, at the same time carrying $Fe(CO)_5$ vapours.

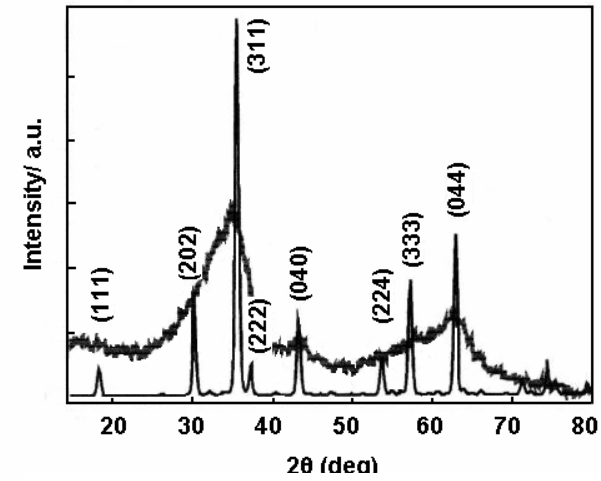

Ftg.2. X-ray diffraction pattern of sample VI showing the characteristic diffraction peaks of γ-Fe2O3 oxide phase

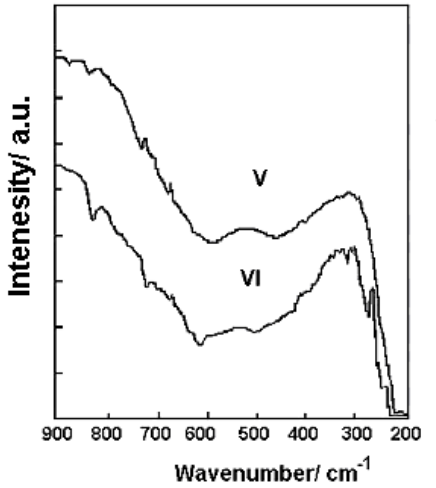

Fig.3. IR spectra of γ-Fe2O3 nanoparticles exhibited by samples V and VI

The flow of ethylene as well as the corresponding carbonyl flow has had relatively high value; simultaneously assuring the efficient heating of the gas mixture (energy transfer by collisions) as well as the transportation of a high quantity of Fe atoms in the volume where the laser induced reaction took place. The result of this last experiment (run VI) was a reddish-brown nanopowders whose X-ray pattern revealed the presence of only one single component, pure γ-Fe_2O_3 (Fig.2) as well as the lack of other oxide phases or contaminants. The large diffraction peaks belonging to γ-iron oxide in Fig.2 suggests very fine particle dimensions. The IR spectrometric analysis of nanopowders with major or total γ- Fe_2O_3 content, i.e. samples V and VI (Fig.3) presents two wide absorption bands which are positioned around 600 and 400 cm^{-1}. These bands are characteristic for disordered maghemite nanoparticles with cubic structure which octahedral positions are randomly distributed.[36]. Most probably, the small differences between the two curves are due to the different crystallinities of the particles which in turn are influenced by their formation temperature: the sample absorptivities at the laser radiation depend on the sensitizer nature and is higher when using SF_6 instead of C_2H_4 in the precursor gas mixture.

Iron/carbon nanocomposite (core-shell nanostructures) Iron nanoparticles are subject to rapid environmental degradation, owing to the very high surface area to volume ratio and high reactivity. This process could be avoided by the encapsulation of metal nanoparticles with carbon/graphitic layers [38, 39], which not only protects the nano-crystals but also could offer new opportunities for the study of their magnetic properties. Much more, because most of the physical properties of interest are those of non-interacting, isolated particles, the coating of nanoparticles represents the best way to preserve their integrity and to prevent their agglomeration by van der Waals forces [40]. We present results of the preparation of iron nano-cores embedded in carbon layers, via a single-step co-pyrolysis method in which the CW CO_2 laser beam irradiates gas-phase reactants [27,28]. The synthesis of Fe-C nanocomposites has been carried out in the flow reactor described in Fig.1. The reactive flow has been partitioned between two concentric nozzles: $Fe(CO)_5$ vapours entrained by C_2H_4 were admitted through the central inner tube while a hydrocarbon mixture including C_2H_2 and C_2H_4 emerged in the reaction cell through an outer concentric tube. The results for two samples synthesized at different temperatures are given below. For CF5 the temperature is higher than for CF6, due to both the increased laser power density and sensitizer concentration.

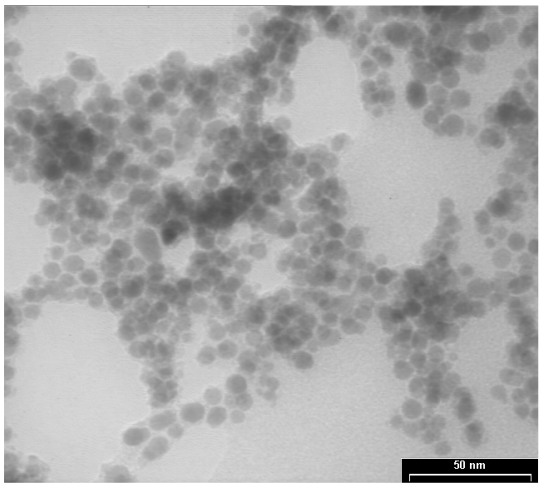

Fig.4 TEM images of Fe-C nanocomposite (sample CF 5)

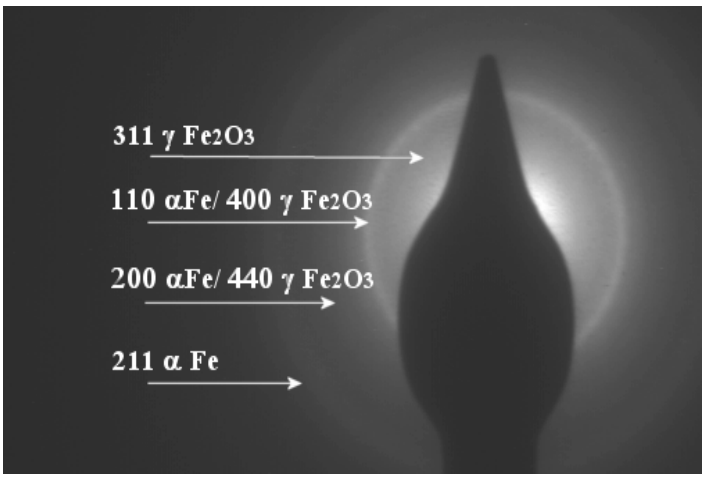

Fig.5 SAED pattern of sample CF5

The TEM characterization of the Fe-C nanocomposites indicates that all samples consist of nanometer-size particles (3-7 nm) showing to a higher or lower extent, the characteristic structure of encapsulated bodies. The even dispersion of particles may be noticed. Almost every particle presents a core (dark contrast) surrounded by a shell/carbon matrix. An example of such an image is presented in Fig.4 (for sample CF5). The SAED pattern referring to TEM image in Fig.4 is shown in Fig.5.The main features point to the presence of α-Fe (as identified by the diffraction rings corresponding to the (110), (311), (200) and (211) hkl planes. Due to overlapping diffraction rings, the presence of an oxidized phase of iron (γ Fe_2O_3), obviously due to the storage in atmosphere, cannot be ruled out.

The structure of particles was observed by HREM analysis. A rather spherical core surrounded by outer carbon sheets is presented in Fig.6. Coalescent features are observed between particles.

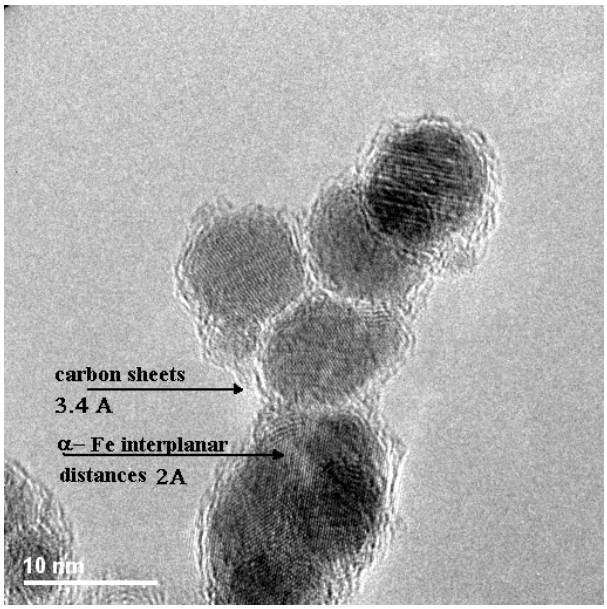

Fig.6 HREM image of CF5 sample

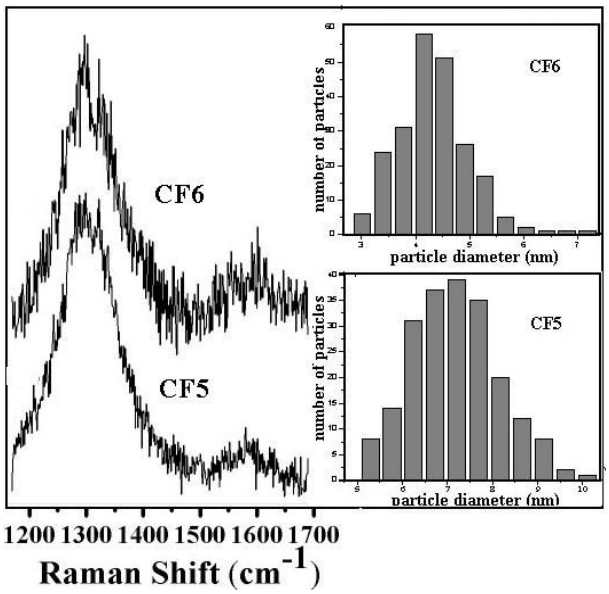

Fig.7. The carbon region of the measured Raman shifts for samples CF5 and CF6: the inserts present de corresponding particle distributions

The carbon region of the Raman measurements of the Fe-C nanocomposite (samples CF6 and CF5) is displayed in Fig.7. Both spectra present rather similar features. A large band centred around 1291 cm^{-1} appears, which could correspond to the D band in graphite. An additional weak but wide band is found at around 1600 cm^{-1}. It is well known that the E_{2g} vibrational mode (the G band) of the graphite lattice appears at 1582 cm^{-1} [41] The band appearing around 1600 cm^{-1} was ascribed in [42] to the defect content of graphite structure. The value of I_D/I_G where I_D is the intensity of the D band and I_G is that of the G band varies inversely with the planar domain size. It is found that the value of I_D/I_G ratio is higher for CF5 than for CF6. An explanation for this behaviour is not yet clear. It may be attributed to an increased disorder and/or some short-range order in the sp^2 domains of the carbon coverage. To the right of Fig.7 two particle size distributions are given: they show that particles of mean diameters 4.2 nm and 7.3 nm were obtained for CF6 and CF5, respectively.

Titanium doped iron oxide nanocomposite. The doping of γ-Fe_2O_3 (maghemite) has attracted attention because of its applications in magnetic recording tape materials. Data concerning doping with tetravalent metals such as titanium [43] are of great interest because of the occurrence of titanomaghemite in nature and because substitution of tetravalent ions can be used to stabilize γ-Fe_2O_3 against transformation to α-Fe_2O_3 (hematite) at elevated temperatures. On the other hand, it was demonstrated that Fe^{3+} doping of titania [44] improves the photocatalytic activity and at higher Fe:Ti ratios superparamagnetic materials may be produced. To our knowledge there is no previous report for titanium doping of irons oxides by the laser pyrolysis method.

Run	C_2H_4 through $TiCl_4$ [sccm]	C_2H_4 through $Fe(CO)_5$ [sccm]	Air [sccm]	P [mbar]
SF16	24	400	165	500
SFT1	68	90	100	400
SF22	250	350	80	800

Table 2. Experimental parameters for the synthesis of titanium doped iron oxide

For the preparation of titanium-doped iron oxides by laser pyrolysis [29], the basic precursors were mixtures of $Fe(CO)_5$ and $TiCl_4$ vapours carried by C_2H_4 through the middle nozzle and air as

oxidizer through the central nozzle (Fig.1). The experimental parameters for some representative runs are given in Table 2. The total Ar flow (for gas confinement and windows cleaning) was 1300 sccm. The main trend distinguishing the three samples is the increasing $TiCl_4$ flow.

X-ray powder diffraction data were obtained for all samples listed in Table 2. The X-ray pattern of the powder obtained in run SF16 (Fig. 8) is shown as an example.

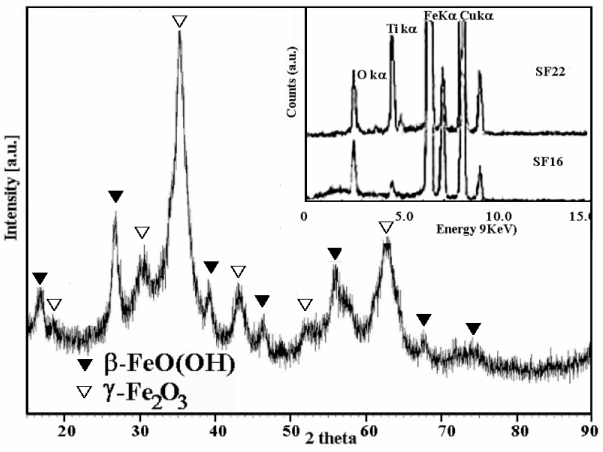

Fig 8 X ray diffraction analysis of sample SF16 and EDAX comparative insert

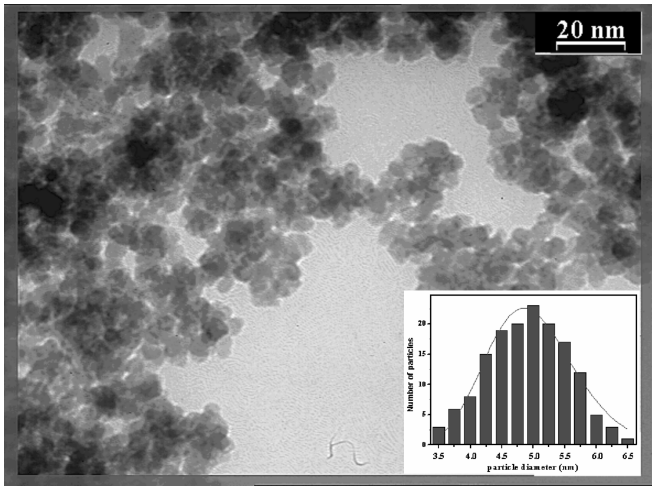

Fig. 9 TEM image of a Ti medium doped sample SF16 and as insert, its particle size distribution

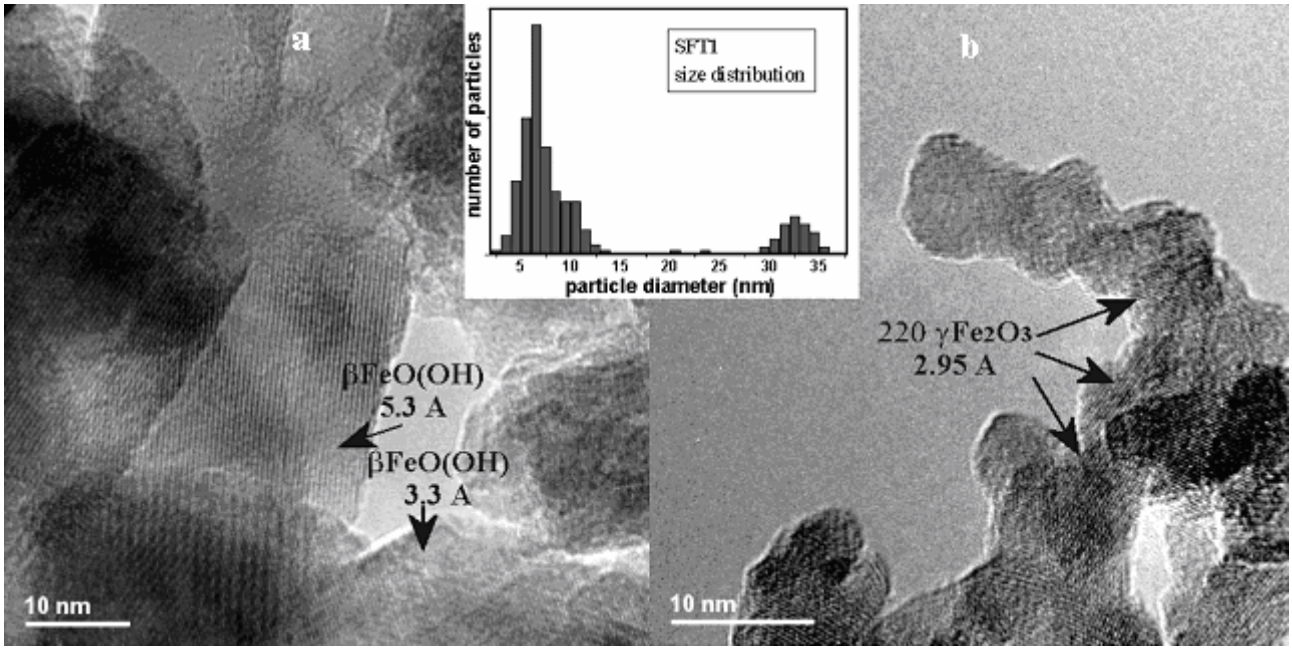

Fig 10 SFT1 HREM images of: a- big particles with identified βFeO(OH) crystalline planes and b- small particles with identified γ-Fe_2O_3 phase; two maxima particle size distribution as insert.

The characteristic peaks of γ-Fe_2O_3 (maghemite) and β-FeO(OH) (akaganéite) are clearly noticeable. The broadened diffraction peaks suggest either very fine particle dimensions or possible contributions from amorphous components or phase impurities. The synthesis of akaganéite is known to require the presence of Cl ions, and therefore the formula should be given as $FeO(OH)_xCl_{1-x}$ [45]. It is obvious that its formation is due to $TiCl_4$ decomposition followed by chlorine atoms release in the reaction atmosphere. By a high increase of $TiCl_4$ flow, the obtained

powders are heavily contaminated by chlorine compounds byproducts (sample SF22). The increase in titanium content of sample SF22 relatively to sample SF16 may be observed by energy dispersive analysis (EDAX) and is depicted as an insert in Fig.8. The TEM image of a Ti medium-doped sample (SF16) is presented in Fig.9. Its particle size distribution (figure insert} indicates a mean particle diameter of about 5 nm. HREM images of a Ti high-doped iron oxide sample (SFT1) are displayed in Fig. 10 a and b. The two images are necessary because the sample exhibited particles with different dimensions. The high-dimension particles (Fig. 10a) present interplanar distances with values close to akaganeite [ICSD 29-129]. The low-dimension particles can be identified as maghemite iron oxide [ICSD 67-119] (Fig. 10b). Superimposed on the two figures is the calculated particle distribution performed on the basis of low magnification TEM image (not presented here) which definitely shows two maxima (around 33 and 7 nm).

It is worthwhile noticing that the incorporation of titanium in the iron oxide lattice leads most probably to the formation of different quantities of titanomaghemite [ICSD 84-1595] whose structure is difficult to determine from x-ray diffraction data due to many coincident values with γ-Fe_2O_3. Magnetic measurements (e.g. Curie temperature) or elemental analysis (such as EELS) are necessary for its identification. It is believed that the oxidation process between titanium magnetite to titanium maghemite is a continuous diffusion solid phase process [46]. Additionally, SFT1 sample scanning with EDAX revealed large variations in the Ti/Fe atomic ratio (between 0-7%), which may express an inhomogeneous Ti incorporation in the sample.

Conclusions

An overview of the laser pyrolysis as method for nanoparticle synthesis is presented. Particular features of iron pentacarbonyl laser pyrolysis in different gas mixtures are underlined. Relationships between synthesis conditions, structure and morphology for some relevant iron-based nanostructures (γ-Fe_2O_3, iron-carbon core-shell particles and Ti-doped γ-Fe_2O_3) have been established.

Acknowledgements.

Special thanks are extended to Dr. Brydson and Dr. David who were involved in different portions of the work described here. The assistance of Prof. Martelli for iron oxide characterization is highly acknowledged. Prof. Ciupina is thanked for interest in this work The authors are grateful to Prof. Rand for providing highly stimulating discussions.

References

[1] W.R. Cannon, S.C. Danforth, J.H. Flint, J.S. Haggerty and R.A. Marra: J. Am. Ceram. Soc. Vol. 65 (1982), p. 324
[2] Y. Suyama, R.M. Marra, J.S. Haggerty and N.K. Bowen: Am. Ceram. Soc. Bulletin Vol. 64 (1985), p.1356
[3] Y. Kizaki, T. Kandori and Y. Fujitani: Jap. J. Appl. Phys. Vol. 24 (1985), p. 800
[4] M. Cauchetier, O. Croix and M. Luce: Adv. Ceram. Mat. Vol. 3 (1988) p. 548
[5] R. Fantoni, E. Borsella, S. Piccirillo, R. Ceccato and S. Enzo: J. Mat. Res. Vol. 5 (1990) p.143
[6] G.W. Rice and R.L. Woodin: J. Mater. Res, Vol. 4 (1989) p. 1538
[7] M. Suzuki, Y. Maniette, Y. Nakata and T. Okutani: J. Am. Ceram. Soc. Vol. 80 (1993) p. 1195
[8] Y.-L. Li, Y. Liang, K.-S. Xiao, F. Zheng and Z.-Q. Hu: Nanostructured Materials Vol. 5 (1995) p.1
[9] R.Alexandrescu, I.Morjan, E.Borsella, S.Botti, R.Fantoni, T.D.Makris, R.Giorgi and S.Enzo: J. Mater. Res.Vol. 6 (1991) p. 2442

[10] F.Huisken, B.Kohn, R.Alexandrescu, S.Cojocaru, A.Crunteanu, C.Reynaud and G.Ledoux: Journal of Nanoparticles Research Vol. 1, (1999) p. 293
[11] G. W. Flynn, C. S. Parmenter and A. M. Wodtke: J. Phys. Chem. Vol. 100 (1996) p. 12817
[12] C. G. Granqvist and R. A. Buhrman: J. Appl. Phys. Vol. 47 (1976), p. 2200
[13] M Ehbrecht., M. Faerber, F. Rohmund, V.V. Smirnov, O. Stelmach and F. Huisken:, Chem. Phys. Lett. Vol. 34 (1993), p. 214
[14] I Voicu, X Armand, M. Cauchetier, N.Herlin and S.Bourcier: Chem. Phys. Lett. Vol. 256 (1996), p. 261
[15] R.Alexandrescu, X. Armand, M. Cauchetier, N. Herlin, S. Petcu and I. Voicu: Carbon Vol. 36 (1998), p. 1285
[16] R.Alexandrescu, E. Borsella, S. Botti, M.C. Cesile, R. Giorgi, S. Martelli and S. Turtu: J. Mater. Sci. Vol. 32 (1997), p. 5629
[17] E. Borsella, R.Alexandrescu, S. Botti, M. Cesile, S. Martelli, R. Giorgi, S. Turtu and G. Zappa: J. Mater. Res. Vol. 12 (1997), p. 774
[18] N. Herlin, I. Bohn, C. Reynaud, M. Cauchetier, A. Galvez and J.N. Rouzaud: Astron. Astrophys. Vol. 330 (1998), p. 1127
[19] R.Alexandrescu, F. Huisken, G. Pugna, A. Crunteanu, S. Petcu, S. Cojocaru, R. Cireasa and I. Morjan: Appl. Phys. A. Vol. 65 (1997), p. 207
[20] R. Alexandrescu, A. Crunteanu, R.E. Morjan, I. Morjan, F. Rohmund, L.K. L. Falk, G. Ledoux and F. Huisken: Infrared Phys. Technol. Vol. 44 (2003), p. 43
[21] H. Hofmeister, F. Huisken, B. Kohn, R. Alexandrescu, S. Cojocaru, A. Crunteanu, I. Morjan and L.Diamandescu: Appl. Phys. A: Mater. Vol. 72 (2001), p. 7
[22] X. Q. Zhao, F. Zheng, Y.Liang, Z.Q. Hu and LY.B. Xu: Mater. Lett. Vol. 21 (1994), p. 285
[23] R. Alexandrescu, S. Cojocaru, A. Crunteanu, I. Morjan, I. Voicu, L. Diamandescu, F. Vasiliu, F. Huisken and B. Kohn: J. Phys. IV France Vol. 9 (1999), p. Pr8-537
[24] S. Martelli, A. Mancini, R. Giorgi, R. Alexandrescu, S. Cojocaru, A. Crunteanu, I. Voicu, M. Balu and I. Morjan: Appl. Surf. Sci. Vol. 353 (2000), p. 154
[25] I. Morjan, R. Alexandrescu, I. Soare, F. Dumitrache, I. Sandu, I. Voicu, A. Crunteanu, E. Vasile, V. Ciupina and S. Martelli: Materials Science and Engineering C Vol.1020 (2002), p. 1
[26] X.-X. Bi, B. Ganguly, G.P. Huffmann, F.E. Huggins, M. Endo and P.C. Eklund: J. Mater. Res. Vol. 8 (1993), 1666
[27] F. Dumitrache, I. Morjan, R. Alexandrescu, B. Rand, V. Ciupina, G. Prodan, I. Voicu, I. Sandu, I. Soare, M. Ploscaru, C. Fleaca, R. Brydson and E. Vasile: Proceedings of SPIE Vol. 4977 (2003), p. 670
[28] F. Dumitrache, I. Morjan, R. Alexandrescu, R.E. Morjan, I. Voicu, I. Sandu, I. Soare, M. Ploscaru, C. Fleaca, V. Ciupina, G. Prodan, B. Rand, R. Brydson and A. Woodword: Diamond Related Materials (2003), in print
[29] F. Dumitrache, B. David, N. Pizúrová, R. Alexandrescu, I. Morjan, O. Schneeweiss, I. Sandu, I. Soare, C. Fleaca, I. Voicu, V. Ciupina and B. Rand: Appl. Phys. A, (2003), to be published
[30] R.Alexandrescu: Appl. Surf. Sci.Vol.106 (1996), p. 28
[31] M.A. Duncan , T.G. Dietz and R.E. Smalley: J. Am. Chem. Soc. Vol. 103 (1981), p. 5245
[32] L. Banares, T. Baumert, M. Bergt, B. Kiefer and G. Gerbe: J. Chem. Phys. Vol. 108 (1998), 5799
[33] K.E. Lewis, D.M. Golden, and G.P. Smith: J. Am. Chem. Soc.Vol. 106 (1984) p. 3905
[34] T. Majima, Y. Matsumoto, and M. Takami, Journal of Photochemistry and Photobiology A: Chemistry Vol. 71 (1993), p.213
[35] X. Q. Zhao, F. Zheng, Y. Liang,, Z.Q. Hu and Y.B. Xu : Mater.Lett. Vol. 21 (1994), p. 285
[36] M.P, Morales, S. Veintemillas-Verdaguer and C.J. Serna : J.Mater.Res. Vol. 14 (1999), p. 3066
[37] S. Veintemillas-Verdaguer, M.P. Morales and C.J.Serna : Mater.Lett. Vol. 35 (1998), p. 2
[38] J. P. Hare, W. K. Hsu, H. W. Kroto, A. Lappas, K. Prassides, M. Terrones and R. M. Walton, Chem. Mater. Vol. 8 (1996), p. 6.

[39] W. Teunissen, F. M. F de Groot, J. Geus, O. Stephan, M. Tence and C. Colliex: J. Catalysis Vol. 204 (2001), p. 169
[38] D.V. Szabo and D. Vollath: Adv. Mater. Vol. 11 (1999), p. 1313.
[39] F. Kokai, K. Takahashi, D. Kasuva, A. Nakayama, Y. Koga, M. Yudasaka and S. Iijima: Appl. Phys. A Vol. 77 (2003), p. 69
[40] T. N. Moroz, E. N. Fedorova, S. M. Zhmoidk, A. G. Mironov, G. M. Rylov, A. L. Ragozin, A. D. Afanasyev and V. I. Zaikobsky: Chemistry for Sustainable Development Vol. 8 (2000), p. 43.
[41] O. Helgason, J.-M. Greneche, F. J. Berry, S. Morup and F. Mosselmans: J. Phys.: Condens. Matter Vol. 13 (2001), p. 10785
[42] Z.-M. Wang, G. Yang, P. Biswas, W. Bresser and P. Boolchand: Powder Technology Vol. 114 (2001), p. 197
[43] E. Murad and J. L. Bishop: American Mineralogist, Vol. 85 (2000), p. 716
[44] W. Xu, D.R. Peacor, W. A. Dollase, R. Van Der Voo and R. Beaubouef: American Mineralogist Vol. 82 (1997), p. 1101.

Functional Nanomaterials for Optoelectronics and other Applications
10.4028/www.scientific.net/SSP.99-100

Recent Developments in the Synthesis of Iron-Based Nanostructures by Laser Pyrolysis: Integrating Structural Analysis with the Experimental Method
10.4028/www.scientific.net/SSP.99-100.181

DOI References
[11] G. W. Flynn, C. S. Parmenter and A. M. Wodtke: J. Phys. Chem. Vol. 100 (1996) p. 12817
doi:10.1021/jp953735c
[22] X. Q. Zhao, F. Zheng, Y.Liang, Z.Q. Hu and LY.B. Xu: Mater. Lett. Vol. 21 (1994), p. 285
doi:10.1016/0167-577X(94)90191-0
[34] T. Majima, Y. Matsumoto, and M. Takami, Journal of Photochemistry and Photobiology A: hemistry Vol. 71 (1993), p.213
doi:10.1016/1010-6030(93)85002-P
[38] J. P. Hare, W. K. Hsu, H. W. Kroto, A. Lappas, K. Prassides, M. Terrones and R. M. Walton, hem. Mater. Vol. 8 (1996), p. 6.
doi:10.1021/cm950339y
[39] W. Teunissen, F. M. F de Groot, J. Geus, O. Stephan, M. Tence and C. Colliex: J. Catalysis ol. 204 (2001), p. 169
doi:10.1006/jcat.2001.3373
[23] R. Alexandrescu, S. Cojocaru, A. Crunteanu, I. Morjan, I. Voicu, L. Diamandescu, F. Vasiliu, F. Huisken and B. Kohn: J. Phys. IV France Vol. 9 (1999), p. Pr8-537
doi:10.1051/jp4:1999867
[34] T. Majima, Y. Matsumoto, and M. Takami, Journal of Photochemistry and Photobiology A: Chemistry Vol. 71 (1993), p.213
doi:10.1016/1010-6030(93)85002-P
[38] J. P. Hare, W. K. Hsu, H. W. Kroto, A. Lappas, K. Prassides, M. Terrones and R. M. Walton, Chem. Mater. Vol. 8 (1996), p. 6.
doi:10.1021/cm950339y
[39] W. Teunissen, F. M. F de Groot, J. Geus, O. Stephan, M. Tence and C. Colliex: J. Catalysis Vol. 204 (2001), p. 169
doi:10.1006/jcat.2001.3373
[41] O. Helgason, J.-M. Greneche, F. J. Berry, S. Morup and F. Mosselmans: J. Phys.: Condens. Matter Vol. 13 (2001), p. 10785
doi:10.1088/0953-8984/13/48/305